Periodica Polytechnica
Civil Engineering

62(1), pp. 126–135, 2018
https://doi.org/10.3311/PPci.10270

Seismic Damage Assessment of an 891 Years Old Historic Masonry Mosque

Muhammet Karaton[1*], Hüseyin Suha Aksoy[1]

RESEARCH ARTICLE

Received 15 November 2015; Revised 27 March 2017; Accepted 02 May 2017

Abstract

Diyarbakir Grand Mosque is one of the oldest and the most significant mosques in the Islamic world and the Mesopotamia. The mosque was heavily damaged due to fire following an earthquake which was predicted 8 magnitude in 1114. It was rebuilt between 1117 and 1125. It is predicted that a great earthquake in the forthcoming years will be occurred in the region. Therefore, conservation and retrofitting works should execute for this 891 years old building. In this study, nonlinear seismic analyses of the main prayer hall of the mosque are performed and damage assessment of it due to a probable great earthquake is determined. Material properties of the mosque are defined by using nondestructive tests. Three level seismic acceleration data are produced by considering seismic characteristics of the region. Damage regions on the mosque are obtained under these earthquake loads. Suggestions about retrofitting of this significant historical mosque are recommended.

Keywords

Diyarbakir Grand Mosque, Sseismic characteristics, nondestructive tests, propagations of damages, conservation work

[1] Engineering Faculty, Civil Engineering Department, Firat University Elazig, Turkey

[*] Corresponding author email: mkaraton@firat.edu.tr

1 Introduction

The most of historical masonry structures in ancient Greek, Mesopotamia, Roman, Chinese, Persian, Egyptian and Incas were built by using construction material as stone, brick or adobe blocks [1]. These structures were constructed according to static loads [2]. Therefore, the structures may be damaged or ruined due to seismic loads [3,4]. Earthquake performances of historical masonry structures must be obtained for carrying to the future and the preserving of them.

Maximum Credible Earthquake (MCE) is used for seismic damage assessment of masonry structures constructed in seismically active areas [5]. Linear seismic analyses of masonry structures show that strong earthquake loads (MCE) can produce tensile stresses which exceed the tensile strength of the lime mortar or strength of adhesion between mortar and stone [6,7]. In such cases, a linear analysis is invalid because tensile cracks will form in the lime mortar or openings will occur between the mortar and stone. The masonry structures can be collapsed due to these cracks. Therefore, nonlinear solutions which include cracking in material and opening/closing behavior of cracks must be used for the seismic analysis of masonry structures.

Many researchers are investigated cracking or damage analysis of masonry stone buildings due to static and/or seismic loading [5–8]. Ramos and Lourenço [5] were investigated nonlinear seismic damage analyses of Pombaline buildings, were rebuilt with novel construction technique after the disastrous 1755 Lisbon earthquake, in Lisbon, Portugal. Material properties of masonry walls were obtained from nondestructive experimental test results. Opening and closing mechanism of obtained cracking zones in the Pombaline buildings were investigated. Some strengthening advices were proposed. Betti and Vignoli [6] investigated static (pushover) and nonlinear seismic analyses of the Basilica of Santa Maria all' Impruneta near Florence in Italy. Masonry units were modelled by using macro elements and a smeared cracking/crushing model were selected for nonlinear behavior of the elements. The results obtained from the nonlinear analyses were compared with the simplified schemes of limit analysis. Brandonisio et al. [7] investigated comparative numerical analyses of four damaged basilica type church for

damage assessment and performance of these churches under the 2009 L'Aquila earthquake loads. These researchers determined that smaller values should be taken than spectrum acceleration values of Italian code for base shear force/total building weight ratio between 20% and 30% in these monumental buildings. Saloustros et al. [8] were studied on church of the Poblet Monastery in Spain. 3D nonlinear analyses of the church were investigated for settlements, reported structural alterations, past earthquakes and gravitational loadings. A continuum damage model was used for nonlinear material behavior. Present damages in the structure are compared with damages zones which obtained by using numerical solutions.

In this study, nonlinear seismic analyses of the Diyarbakir Grand Mosque are performed. A smeared crack model is used for the nonlinear material behavior which includes tensile cracking and compressive crushing effect. Homogenized material properties are used for stone and mortar of the mosque. Schmidt and ultrasound test for stone material and Sulfuric acid mass loss test for mortar are performed for determination of the material properties. Seismic acceleration data are produced for three different levels (D1, D2 and D3) considering the seismic characteristics of the region where the mosque is located [9]. Damages in Diyarbakır Grand Mosque under the D1 earthquake level cannot be observed, but cracking and damages are obtained under D2 and D3 earthquake levels.

2 Numerical Modelling of Masonry Units

The masonry structures are constructed with/without mortar and stone/brick materials. Numerical modeling of the structures is quite complex due to the interaction of these materials. For the numerical modeling of the masonry, micro, simplified micro and macro modelling are used (Fig.1). In the micro modelling, stone/brick, mortar materials and interface elements are separately modeled. Interaction of the materials are taken into account in the numerical solutions. In simplified micro model, dimensions of stone/brick are extended as much as half thickness of the mortar. Thus, stone/brick units with mortar are defined in the finite element mesh and interface elements are used between these units. In the macro modelling, stone/brick and mortar is considered as a homogenized domain. Effective material properties are obtained for the homogenized domain [2,5,10].

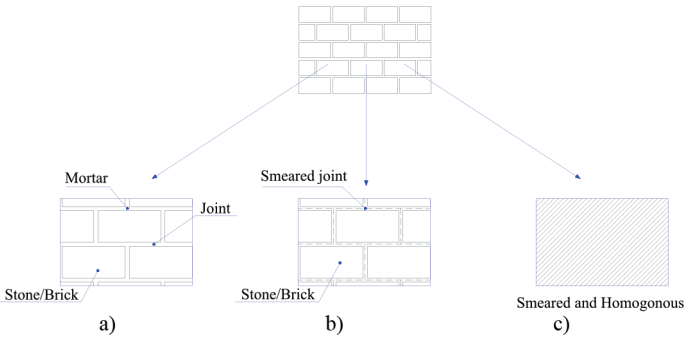

Fig. 1 a) micro, b) simplified micro and c) macro modeling of the masonry walls (Proske and Gelder 2009).

In this study, a smeared crack model, includes the strain softening, cracking and crushing behaviors of material, is used for nonlinear behavior of the masonry stone walls. This model is three parameters model which a special case of five parameters model of William and Warnke [11–13]. Zeinkiewicz and Taylor [13] were stated that the model can be used for the brittle materials. This model is used effectively for macro modeling of the masonry structures [5–8].

3 Determination Material Properties of Diyarbakir Grand Mosque

In this section, Diyarbakir Grand Mosque is presented and material properties of the mosque are defined by using nondestructive tests. Homogenized material properties of the mosque are obtained by using these test results.

3.1 Diyarbakir Grand Mosque

Diyarbakir Grand Mosque is one of the oldest mosques in the whole Islamic world. The date of the construction of this structure which located in the Diyarbakır city center is unknown. Diyarbakir Grand Mosque, fell into ruin in time, was rebuilt by order of Sultan Malik Shah of Seljuk Empire in 1091. The building was heavily damaged due to an earthquake and following fire in 1114. Atabek Inaloglu Abu Mansur Ilaldi rebuilt the mosque between 1117 and 1125. From this date, the building has been minor restorations for present day [14]. Courtyard of the mosque is 63 meters long by 30 meters wide and buildings of the mosque are located around the courtyard. Main prayer hall was located at entire south wall of the courtyard (Figure 2). Additional buildings have been constructed until today. These buildings are Mesudiye Madrasah (1193) and Zinciriye Madrasah (1189) which located at north and west of the courtyard, respectively (Fig. 3.a). Due to cultural and historical importance of the mosque, a conservation work should carry out, and damage assessment of this historical building must be established by using advanced numerical techniques.

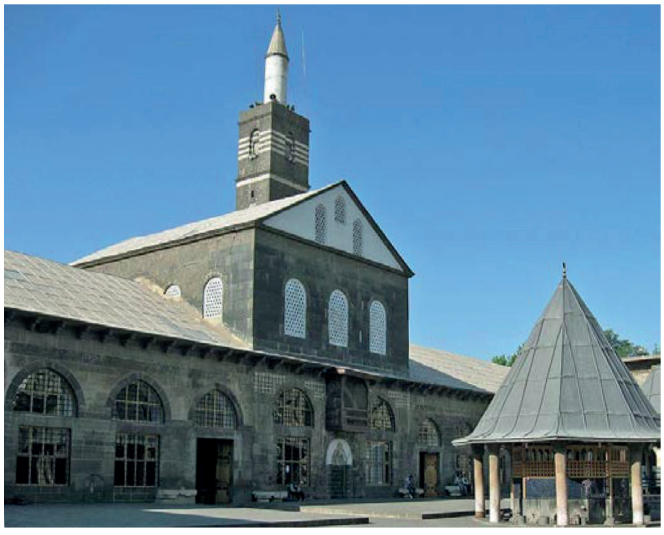

Fig. 2 General view of Diyarbakır Grand Mosque.

In this study, nonlinear seismic analysis of the main prayer hall is performed. Detailed plan of main prayer hall are shown in the Fig. 3.b and c. The building have rectangular plan (75×18.75 m) and it is consist of three parts which central, east and west halls. Central hall and east/west halls have 9.82 m and 5.69 m height, respectively. The east and west halls are consist of three aisles.

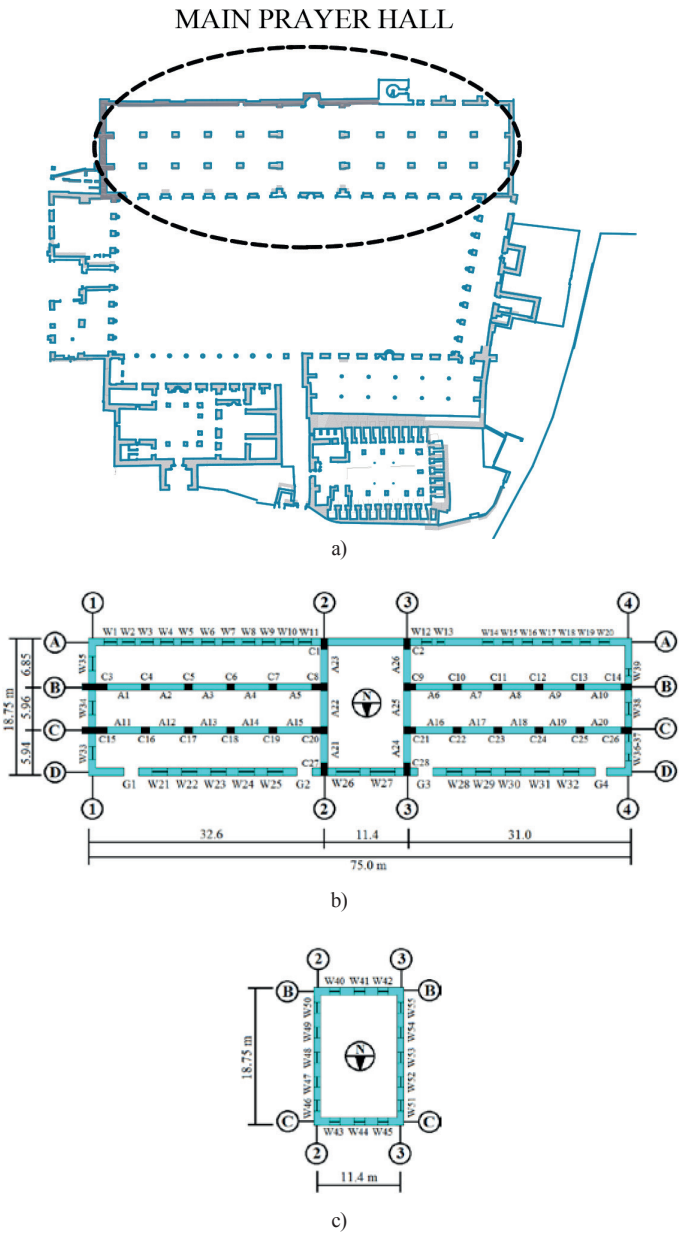

Fig. 3 a) Plan layout of Diyarbakır Grand Mosque, b) Ground and c) first floor plans of main prayer hall.

3.2 Determination of Material Properties of the Mosque

Diyarbakir Grand Mosque is mainly constructed with three class masonry wall. Arches and piers are consists of only ashlar vesicular basalt stones. This basalt type was chosen because it is easy to carve. The outer walls of the mosque were built with massive basalt stone. Foundation stones were also constructed with massive basalt stone. These stones have between 25–110 cm dimensions. Masonry units are constructed by mortar which have between 2.5–6.0 cm dimensions. In this research, properties of construction materials of the mosque are defined by using the results of Schmidt hammer, ultrasound and sulfuric acid mass loss tests.

3.2.1 Mechanical Properties of Stone Material

In this section, mechanical properties of stone material are defined by using Schmidt hammer and ultrasound test results. Schmidt L type hammer rebound values are obtained from 375 different points for outer walls and columns according to Poole and Farmer [15,16]. Ultrasound speeds are measured at 8 different columns, and these measurements are performed by using Proceq pundit with pressure and shear wave transducers. Mass density of outer walls and columns are taken as 2.85 and 2.28 t/m^3, respectively [17].

The ultrasound test results can be seen at Table 1. Average value of elasticity modulus and Poisson ratio are obtained as 26129 MPa and 0.34, respectively. Elasticity modulus of outer walls are determined by using previously proposed empirical studies based on Schmidt rebound values. These empirical studies are firstly calibrated with elasticity modulus obtained from ultrasound test results of columns.

Table 1 Ultrasound Test Results of columns

Location	V_p (m/s)	V_s (m/s)	ν	E(MPa)
C1	4323	2097	0.35	26993
C3	4059	2214	0.29	28795
C7	4323	1963	0.37	24075
C9	4526	2190	0.35	29462
C12	4091	2072	0.33	25988
C14	4101	2044	0.33	25429
C15	4371	2027	0.36	25537
C17	4194	1909	0.37	22756
	Mean		**0.34**	**26129**

Table 2 Elasticity modulus of columns and outer walls determined from empirical relationships by using the rebound values

	Columns	Outer walls
N (Rebound)	**48910**	**55450**
E (MPa) [18]	44130	62820
E (MPa) [19]	21590	31810
E (MPa) [20]	8310	11520
E_{mean}(MPa)	**24674**	**35384**

In Table 2, determined elasticity modulus values of columns are given. Mean of elasticity modulus of columns is 24674 MPa (Table 2). This value is approximately equal to elasticity modulus of columns obtained from ultrasound test results. Thus, mean elasticity modulus of outer walls is calculated as 35384 MPa by using same relationships (Table 2). Mean uniaxial compressive strength of vesicular and massive basalts of Diyarbakır region according to laboratory test results were defined as 51.76 and 89.10 MPa, respectively [17]. Mean

uniaxial compressive strength of columns and outer walls from empirical relationships by using the rebound values are calculated as 52.883 and 87.000 MPa, respectively (Table 3).

Table 3 Uniaxial compressive strength of columns and outer walls determined from empirical relationships by using the rebound values

	Columns	Outer Walls
γ (t/m^3)	2.28	2.85
N (Rebound)	**48.910**	**55.45**
f_c (MPa) [21]	48.938	115.380
f_c (MPa) [22]	42.123	62.897
f_c (MPa) [18]	40.597	59.713
f_c (MPa) [19]	67.809	107.178
f_c (MPa) [23]	64.947	89.825
$f_{c,mean}$ (MPa)	**52.883**	**87.000**

Table 4 Uniaxial compressive strength of columns and outer walls determined from empirical relationships by using elasticity modulus

	Columns	Outer Walls
E (MPa)	26129	35384
f_c (MPa) [18]	72.498	105.551
f_c (MPa) [19]	41.359	77.371
$f_{c,mean}$ (MPa)	56.929	91.461

Furthermore, mean uniaxial compressive strengths of columns and outer walls obtained from empirical relationships by using elasticity modulus are also calculated as 56.929 and 91.461 MPa, respectively (Table 4). Thus, mean of these two results for uniaxial compressive strengths of column and outer walls are obtained as 54.906 and 89.231 MPa, respectively. These values are approximately similar to test results of Kahveci [17]. Compressive/tensile strength ratio of vesicular and massive basalts of Diyarbakır region is determined as approximately 7.0 [17]. Tensile strength of columns and outer walls are calculated as 7.844 and 12.747 MPa, respectively, by using this ratio.

3.2.2 Mechanical Properties of Mortar

A mortar sample are taken from main prayer hall for determination of mortar material properties of Diyarbakir Grand Mosque. Sulfuric acid mass loss test are performed on this sample, results are given in Table 5. Volumetric lime/sand ratio is determined as 1/2.5.

Karaveziroglou et al. [24] were investigated on mechanical properties of Byzantine and Ottoman mortars in Thessaloniki. Mortar samples, have different coarse or fine aggregate/Lime-pozzolan mixing ratios, were produced according to Byzantine and Ottoman mortars. The mixing ratio of K4, K5 and K19 samples are consistent with mortar's mixing ratio of the Diyarbakir Grand Mosque. Mean compressive, tensile strength, density and elasticity modulus of these samples are obtained as 0.759 MPa, 0.274, 1.670 t/m3 and 1845 MPa, respectively.

Table 5 Mixture ratio lime: mortar

Total weight gr)/ Volume (cm^3)	Fine aggregate weight (gr)/(cm^3)	Coarse aggregate weight (gr) /(cm^3)	Lime Weight (gr)/(cm^3)	Acid loss (%)
42.900/25.689	1.260/0.485	29.830/11.47	10.98/4.774	27.5

3.3 Determination of Mechanical Properties of Homogenized Masonry Units

Stone masonry walls are a composite material which consist of stone and mortar. For this reason, composite material theory is used for determination of homogenized material properties of masonry units. Proske and Gelder [2] were proposed empirical equations for homogenization of masonry units. This relation is based on compressive strength of mortar and stone;

$$f_{c,mas} = a\, f_{c,st}^{b}\, f_{c,mo}^{c} \tag{1}$$

where $f_{c,mas}$ is compressive strength of homogenized masonry unit, a is classification coefficient of masonry unit. b and c are participation rate of stone/brick and mortar, respectively. Eq.(1) proposed in Eurocode 6 [25] as,

$$f_{c,mas} = 0.4\, f_{c,st}^{0.65} . f_{c,mo}^{0.25} (MPa) \tag{2}$$

In this study, uniaxial compressive ($f_{c,mas}$) and tensile strength ($f_{t,mas}$) of masonry units are calculated by using Eq.(2). Density (γ_{mas}) and Poisson ratio (v_{mas}) of masonry units is also calculated as [26],

$$\gamma_{mas} = \gamma_{st} . V_{st} + \gamma_m . V_m \tag{3a}$$

$$v_{mas} = v_{st} . V_{st} + v_m . V_m \tag{3b}$$

where, V_{st} and V_m are volumetric participation rate of stone and mortar, respectively. Elasticity modulus (E_{mas}) of masonry unit is taken as $E_{mas} = 1000\, f_{c,mas}$. Due to limit loading cases, elasticity modulus values are reduced by 0.6 coefficient [25]. Homogenized material properties of column and outer walls can be seen in Table 6. In this table, $f_{mas,c}$, $f_{mas,t}$, E_{mas}, ρ_{mas} and v_{mas} are compressive strength, tensile strength, elasticity modulus, mass density and Poisson ratio of related masonry unit, respectively.

Table 6 Homogenized material properties of three class masonry units.

Material properties	Columns/foundation	Outer walls
$f_{c,mas}$ (MPa)	5.045	6.918
$f_{t,mas}$ (MPa)	1.104	1.514
E_{mas} (MPa)	3027	4151
ρ_{mas} (ton/m^3)	2.22	2.73
v_{mas}	0.33	0.33

4 Producing of Synthetic Earthquakes Data for the Location of the Mosque

Turkey is located in one of tectonically active region of the Earth and it has two major fault zones which are North Anatolian Fault Zone (NAFZ) and the East Anatolian Fault Zone (EAFZ).

These fault zones can be seen in Fig. 4. EAFZ, is a strike slip fault, starts from Karlıova triple junction and extends to Türkoğlu triple junction (about 435 km length). Shear velocity on EAFZ is measured between 9-15 mm/year [27,28]. Seismic energy are accumulated on three seismic gaps, Andırın, Türkoğlu and Lake Hazar, on the EAFZ since 1900. In the future, destructive earthquakes on these seismic gaps are expected. The Diyarbakir Grand Mosque was heavily damaged and ruined due to an earthquake and following fire in 1114. The earthquake was happened Maras, Urfa, Harran regions and it is assumed that has 8 magnitudes [29]. It is predicted that this important building will be affected due to strong earthquakes on the EAFZ.

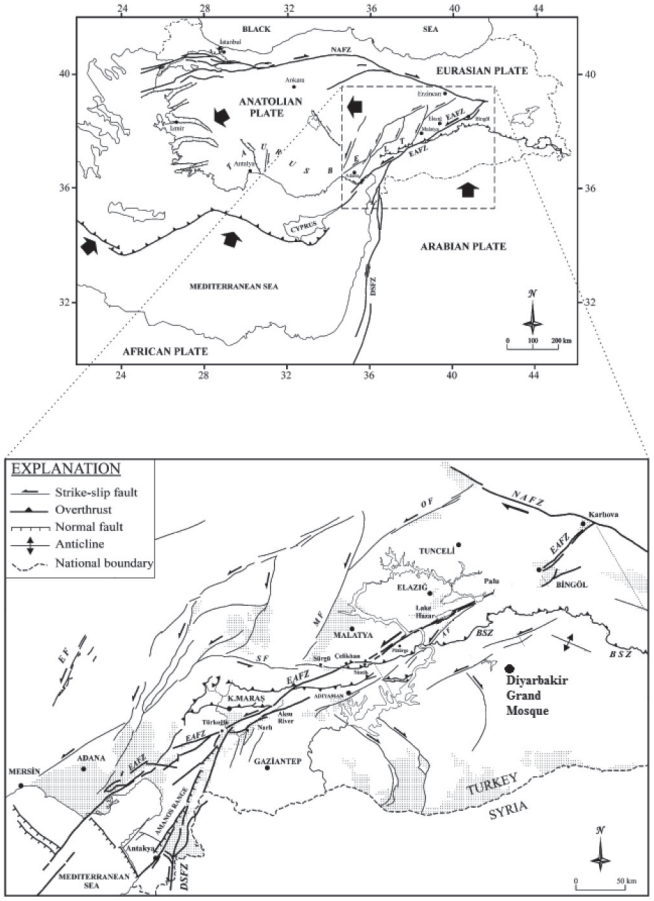

Fig. 4 East Anatolian Fault Zone and the Diyarbakir Grand Mosque [30].

In this study, seismic acceleration data are produced for three different levels (D1, D2 and D3) considering the seismic characteristics of the region (DLH 2007). D1, D2 and D3 earthquake levels indicate the probability of exceedance 50%, 10% and 2% in 50 years, respectively. Return periods of D1, D2 and D3 earthquake levels are 72, 475 and 2475 years, respectively. Properties of spectrum acceleration graphs (Fig. 5) are determined by using latitude and longitude of the Diyarbakır Grand Mosque according to DLH [9]. These spectrum acceleration graphs are used to produce data of synthetic acceleration. This data producing procedure is achieved by using SeismoArtif [31] program. Synthetic acceleration-time graphs of these earthquake levels can be seen in Fig. 6. Absolute maximum acceleration amplitude of D1, D2 and D3 earthquake levels are obtained as 0.072g, 0.143g and 0.251g, respectively. These seismic loadings are produced for one direction. Thus, solutions are separately obtained for each directions. It is seen that damage intensities obtained in the mosque in y direction are greater than the other two directions (x and z, vertical). Therefore, only this direction solutions are given in this research.

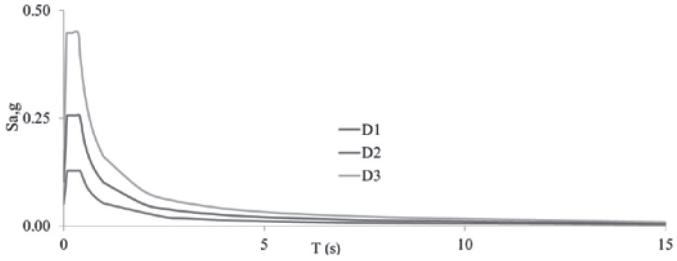

Fig. 5 Target spectrum acceleration graphs of D1, D2 and D3 earthquake levels.

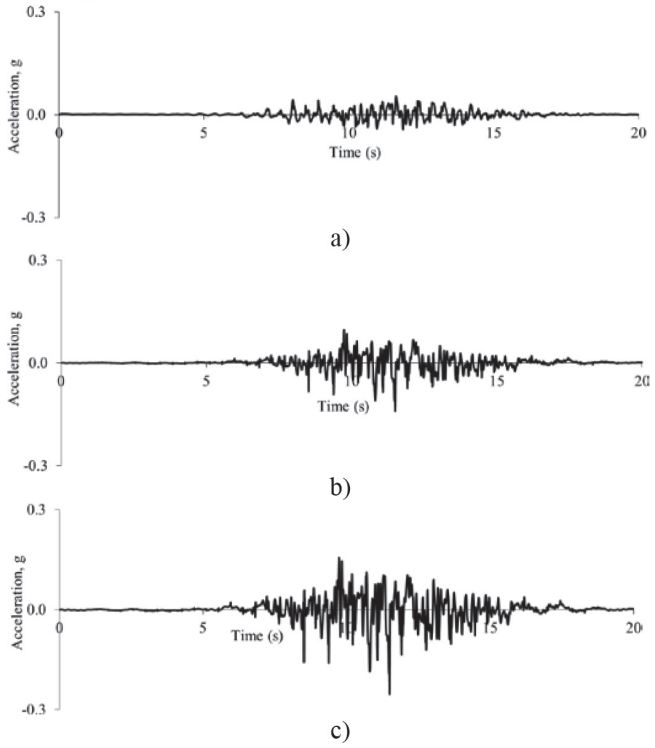

Fig. 6 Acceleration-time graphs of synthetic a) D1, b) D2 and c) D3 earthquake levels.

5 Numerical Analyses of Diyarbakır Grand Mosque

Three dimensional solid finite elements are used for nonlinear analyses of the building. Finite element mesh of the mosque is shown in the Fig. 7. 31029 nodal points and 14635 solid elements are used in the finite element mesh. Finite element models on B, C, 2 and 3 axes are divided two or three finite elements in direction of thickness. Damage intensities in these walls are greater than other walls. Finite element model of other walls have one element in direction of thickness. Cracking or crushing effects are calculated at each one integration point. Thus, in the calculations, one element is divided two region in spite of a wall have one element in direction of thickness.

Fixed smeared crack model which includes tensile cracking and compressive crushing, is selected for nonlinear behavior of homogenized masonry. Nonlinear seismic analyses of the building are obtained by using produced synthetic acceleration data which is effected in the north-south direction of the mosque. Damping in the building is assumed as being proportional to the tangent stiffness and mass matrices. It is provides a critical viscous damping ratio of 5% in fundamental vibration modes of the building with no cracking. Predicted-corrected form of the Generalized-α algorithm for dynamic integration method is used for the solutions. Integration time step is selected as 0.001 sec. due to the cracking and crushing effects in the masonry domain. ANSYS finite element program is used for the solutions [12]. In this study, probable damage zones, displacement responses and seismic performances of the building are investigated.

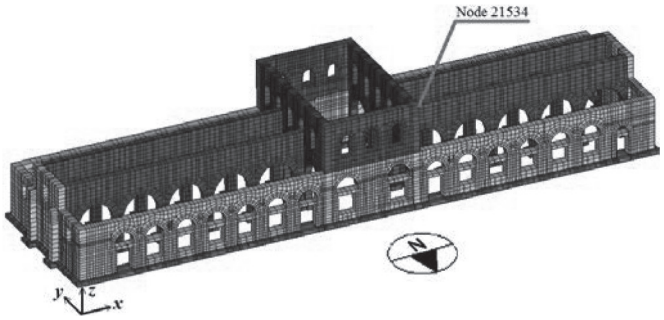

Fig. 7 Finite element mesh of the Diyarbakır Grand Mosque.

5.1 Nonlinear seismic analysis of the mosque under D1 earthquake level

Time history graph in *y* (cross) direction of 21534 node can be seen in Fig. 8. Absolute maximum displacement value is obtained as 2.52 mm. No damage are observed in Diyarbakır Grand Mosque under the D1 earthquake level.

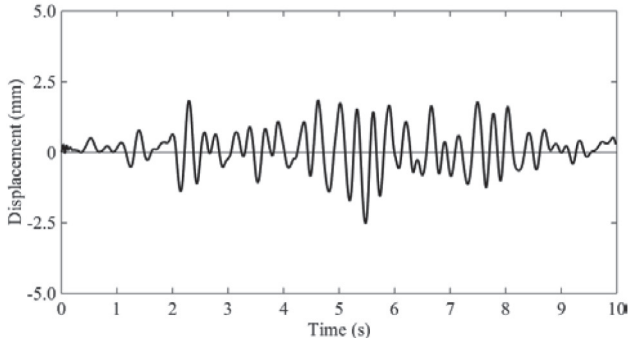

Fig. 8 Time history graph in *y* (cross) direction of 21534 node for D1 earthquake level.

5.2 Nonlinear seismic analysis of the mosque under D2 earthquake level

In Fig. 9, time history graph in y (cross) direction of 21534 node of the mosque is given under D2 earthquake level. As seen in this figure, absolute maximum displacement value is determined as 4.42 mm. Ground and first floor plans of Diyarbakır Grand Mosque are given in Fig. 3.b and c. Cracking zones are observed in the mosque under D2 earthquake level. These zones are investigated for 1, 2, 3, 4, A, B, C and D axes of the mosque. Five cracking zones are observed in B, C, 2 and 3 axes and these damages can be seen in Fig. 10 and 11 at t = 4.97, 5.55 and t = 10.00 sec. First cracking zone in Diyarbakır Grand Mosque is formed at intersection region of 3 axis with C axis (under W52 window) at 4.97 sec. as seen in Fig. 10.a. New cracking region is observed lower side of W47 window which located on intersection region of 2-C axes at t = 5.52 sec. (Fig. 10.b). Additional crack regions are obtained upper side of C9, C21, C8, C20 columns at 5.54 and 5.59 sec., respectively (Fig. 10.b, 10.c, 11.a and 11.b). Base region of C6 column is cracked at 5.55 sec. (Fig. 11.a). Propagations and extensions of the cracking regions are observed until t = 10.00 sec. as seen in Fig. 10.b and d. Seismic analysis of the mosque under the earthquake is converged for all solution steps.

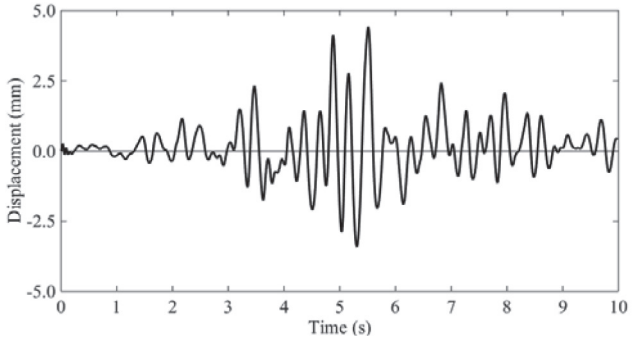

Fig. 9 Time history graph in y (cross) direction of 21534 node for D2 earthquake level.

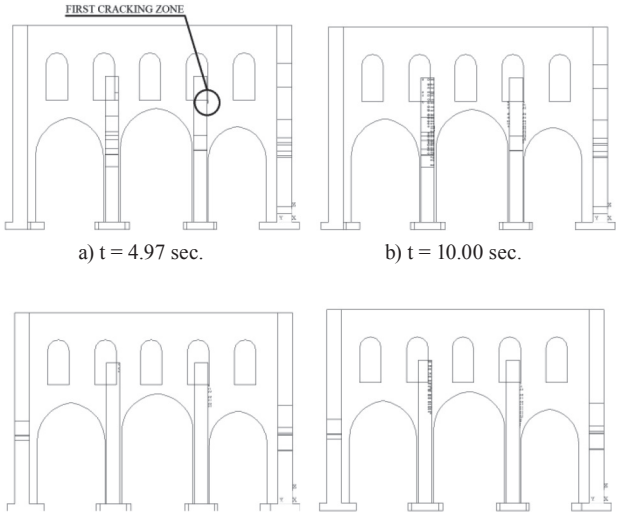

Fig. 10 Cracking zones at a) t = 4.97 sec. for 3 axis, b) t = 10.00 sec. for 3 axis, c) t = 5.55 sec. for 2 axis and d) t = 10.00 sec. for 2 axis under D2 earthquake level.

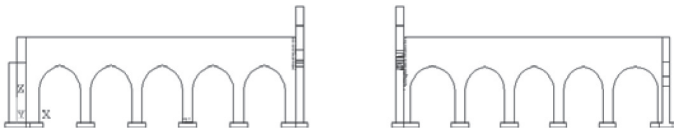

a) Cracking zones in B axis at t = 10.00 sec.

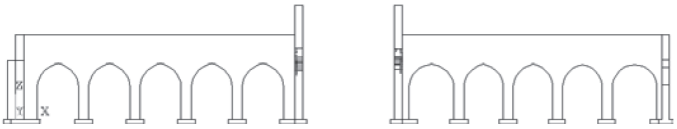

b) Cracking zones in C axis at t = 10.00 sec.

Fig. 11 Cracking zones on a) *B* and b) *C* axes for D2 earthquake level.

5.3 Nonlinear seismic analysis of the mosque under D3 earthquake level

Time history graph in *y* (cross) direction of 21534 node of the mosque under D3 earthquake level is given in Fig. 12. As seen in this figure, absolute maximum displacement value is determined as 66.2 mm. Damage (cracking and crushing) zones at 1, 2, 3, 4, A, B, C D axes of the mosque and local collapse mechanisms at 2, 3, B axes are observed in the mosque under D3 earthquake level. These damage zones and collapse mechanisms are given in Figs. 13–22.

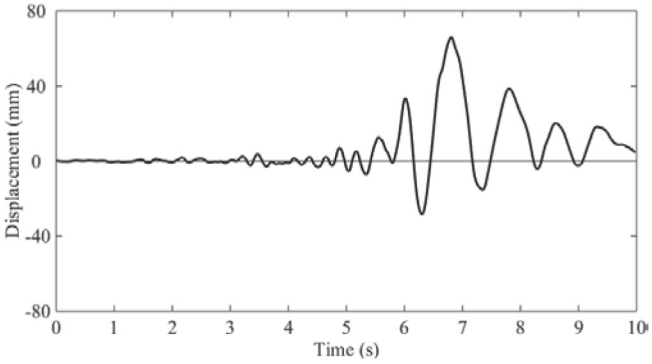

Fig. 12 Time history graph in *y* (cross) direction of 21534 node for D3 earthquake level.

First cracking zone in Diyarbakır Grand Mosque is formed on intersection region of 3 axis with C axis at 3.93 sec. as seen in Fig. 15.a. In 1 axis, cracking is initiated on intersection region of 1 axis and B axis at 4.87 sec. as seen in Fig. 13.a. This cracking region is occurred due to movement of B axis in direction of north–south. Propagations of this cracking zone are observed from this time to 10 sec. (Fig. 13.b).

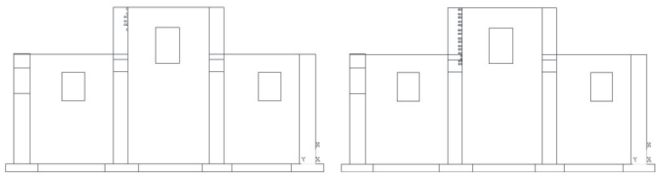

a) t = 4.87 sec. b) t = 10.00 sec.

Fig. 13 Cracking zones on 1 axis for D3 earthquake level.

Cracking zones on 2 axis are seen in intersection regions of 2-C axes at t = 4.58 sec. (Fig. 14.a), after this moment, new cracking zones are occurred in base regions of C1 column, in region between A21 arch-C27 column, in lower part of W50 window, in upper and base regions of C8 column at t = 4.95 sec. (Fig. 14.b). In between t = 4.95 sec. to 5.56 sec., additional cracking zones are seen in region between A23 arch-W50 window, in base regions of C20 and C27 columns and in lower part of W46 window, in upper part of W50 window and in region between A22 arch-C20 column (Fig. 14.c). These cracking zones are propagated and extended between t = 5.56–10.00 sec. However, some crushing regions are observed in these cracking zones until t = 10.00 sec. (Fig. 14.d). It is assumed that regions between these crushing zones are reached to local collapse mechanism.

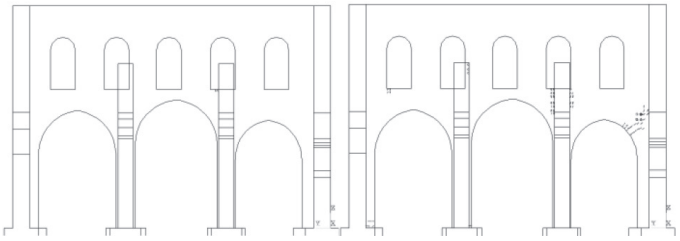

a) t = 4.58 sec. b) t = 4.95 sec.

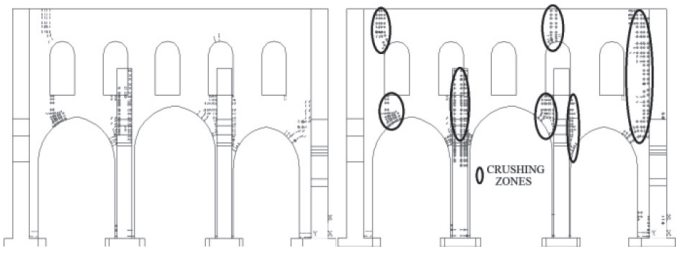

c) t = 5.56 sec. d) t = 10.00 sec.

Fig. 14 Cracking zones on 2 axis for D3 earthquake level.

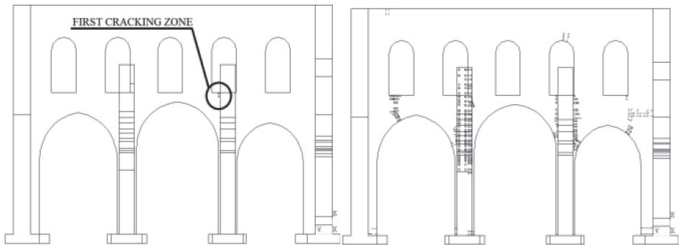

a) t = 3.93 sec b) t = 5.54 sec.

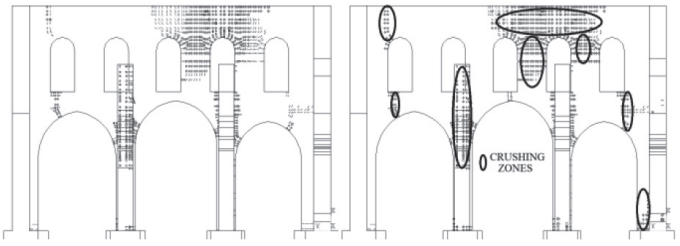

c) t = 5.63 sec. d) t = 10.00 sec.

Fig. 15 Cracking zones on 3 axis for D3 earthquake level.

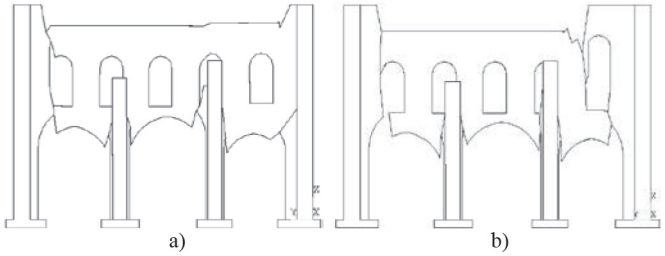

a) b)

Fig. 16 Collapse mechanism a) 2 axis and b) 3 axis for D3 earthquake level.

As mentioned above, first cracking zone on 3 axis are seen Fig. 15.a. Additional cracking zones are occurred in base regions of C2 and C9, in region between A24 arch-W51 window and in lower part of W55 window at t = 4.88 sec. Damage zones are also observed in base region of C21 column, in upper region of C9 column, in base region of C28 column and in lower part of W51 window at t = 4.90, 4.93, 5.02 and 5.05 sec., respectively. New cracking zones are obtained in upper regions of W55 and W52 windows at t = 5.54 sec. (Fig. 15.b), after this time, some propagations and extensions are observed until t = 5.62 sec. However, at t = 5.63 sec., sudden crack propagations are seen in regions between W51–W52 and W52–W53 windows (Fig. 15.c). Until t = 10.00 sec., some crushing regions are observed in signed areas which given in Fig. 15.d. It is assumed that regions between these crushing zones are reached to local collapse mechanism. Local collapse mechanism of 2 and 3 axes are given in Fig. 16. This mechanism are developed due to movement in direction of north-south of right and left aisle walls which neighbor to middle aisle. This movement mostly effect to intersection regions of C1, C8, C20 and C27 columns with extrados of A21, A22 and A23 aches. Similar response are observed at 3 axis.

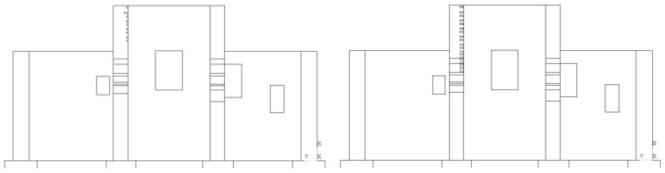

a) t = 4.85 sec b) t = 10.00 sec

Fig. 17 Cracking zones on 4 axis for D3 earthquake level.

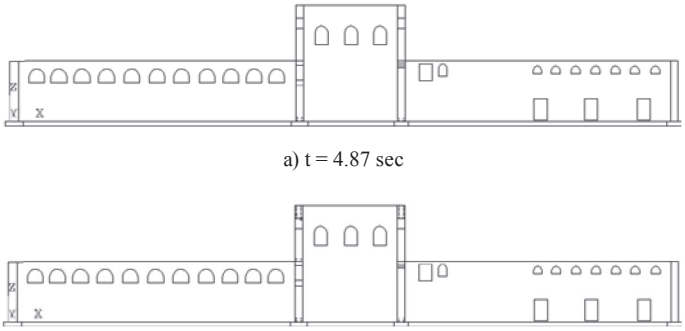

a) t = 4.87 sec

b) t = 10.00 sec

Fig. 18 Cracking zones on A axis for D3 earthquake level.

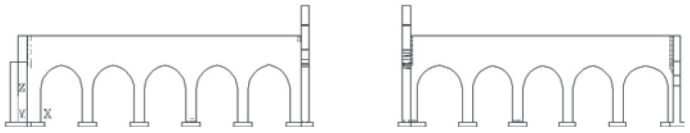

a) t = 4.95 sec.

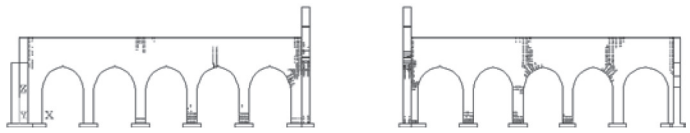

b) t = 6.90 sec.

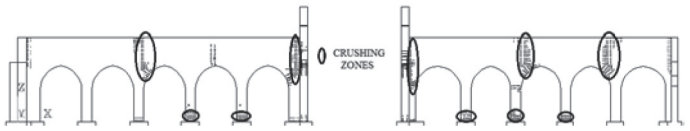

c) t = 10.00 sec.

Fig. 19 Cracking zones on *B* axis for D3 earthquake level.

In 4 axis, cracking is initiated in intersection region of 4 axis and B axis at 4.85 sec. as seen in Fig. 17.a. Some propagations and extensions in this cracking zone are observed from this time to 10 sec. (Fig. 17.b). In A axis, cracking zones are occurred in base regions of C1 and C2 columns at 4.87 sec. as seen in Fig. 18.a. Afterward, additional cracking zones are observed in middle and upper regions of C1 column and in upper region of C2 column until t = 10 sec. (Fig. 18.b).

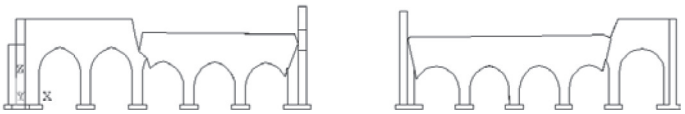

Fig. 20 Collapse mechanism B axis for D3 earthquake level.

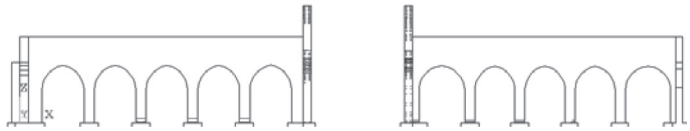

a) t = 5.65 sec.

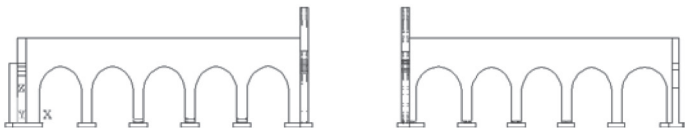

b) t = 10.00 sec.

Fig. 21 Cracking zones on C axis for D3 earthquake level.

Cracking zones on *B* axis are seen in intersection regions of 4-B axes at t = 4.85 sec., after this moment, new cracking zones are occurred in intersection regions of 1-B axes at t = 4.87 and base regions of C8 and C9 columns at t = 4.88 sec. Additional cracking zones are seen in base regions of C6 and C11 columns, in intersection regions of 2-B and 3-B axes at t = 4.95 sec. (Fig. 19.a). New damage zones are occurred in base regions of C7 and C10 columns at t = 5.55, 5.56 sec., respectively. Intersection region of A5 arch-C8 column and base region of C5 column are cracked at t = 5.63 sec. Furthermore, keystone region of A4 arch and base region of C12 column are cracked at t = 6.02 sec.

Upper regions of A8, A9 and A3 arches are damaged at t = 6.41, 6.54 and 6.90 sec., respectively (Fig. 19.b). These cracking zones are propagated and extended between t = 6.90–10.00 sec. However, some crushing regions are observed in these cracking zones until t = 10.00 sec. These crushing regions are signed in Fig. 19.c. It is assumed that areas between these crushing regions are reached to local collapse mechanism. Local collapse mechanism of B axis can be seen in Fig. 20. The mechanism are developed due to movement of central hall in direction of north-south. This collapse mechanism is occurred in between C5 column-A3 arch with C8 column-A5 arch and in between C9 column-A6 arch with C12 column-A8 arch.

In C axis, cracking zones are seen in intersection regions of 3-C axes and of 2-C axes at t = 3.93 and 4.58 sec., respectively, after this moment, the cracking zones are extended and propagated until t = 5.60 sec. New damage zones are occurred in base regions of C17, C18, C19, C22, C23 and C24 columns between t = 5.60–5.65 sec. (Fig. 21.a). Propagations of the damage zones are observed until t = 10.00 sec. (Fig. 21.b).

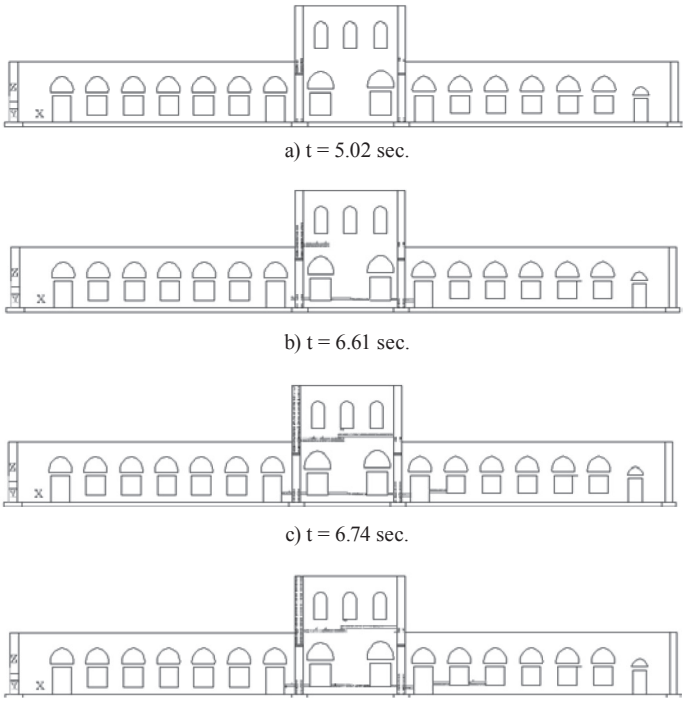

a) t = 5.02 sec.

b) t = 6.61 sec.

c) t = 6.74 sec.

d) t = 10.00 sec.

Fig. 22 Cracking zones on *D* axis for D3 earthquake level.

6 Conclusions and suggestions

Diyarbakir Grand Mosque is one of the oldest mosques in whole Islamic world and it is one of the most significant mosques in Mesopotamia. The building was heavily damaged due to an earthquake and following fire in 1114. It predicted that has 8 magnitudes. It was rebuilt between 1117 and 1125. From this date, the building has been reaching with minor restorations to present day. It is predicted that the building will be affected by a strong earthquake on the EAFZ. Due to cultural and historical importance of it, a conservation work should carry out, and damage assessment of this historical building must be established.

In this study, material properties of the mosque are defined by using non-destructive tests (Schmidt hammer, ultrasound and Sulfuric acid mass loss tests). Seismic acceleration data are produced for three different levels (D1, D2 and D3) considering seismic characteristics of region where the mosque is located. Nonlinear seismic analyses of the main prayer hall of the mosque are performed. Seismic performance of the hall are investigated under these earthquake levels.

Cracking zones are determined for 1, 2, 3, 4, A, B, C and D axes of the mosque. When no damage is obtained under the D1 earthquake level in Diyarbakır Grand Mosque, cracking and damages are observed under D2 and D3 earthquake levels. Five cracking zones in the mosque under D2 earthquake level are obtained. Four cracking zones are observed in intersection regions of 2 and 3 axes with B axis and in intersection regions of 2 and 3 axes with C axis. The other cracking zone is seen in base region of C6 column. No important propagations of the cracks are take placed until last numerical solution. The mosque is remains stable for all solution steps.

When investigating of cracking/crushing zones are occurred in the mosque under D3 earthquake level, cracking zones are observed at all axes. The nonlinear analysis of the mosque are converged for all solution steps in spite of heavy damages. Damages in B, C, 2 and 3 axes are propagated to wider regions than the other axes. Large relative displacements in these regions are occurred due to low rigidity of structural elements between B and C axes with 1–2 and 3–4 axes of the mosque in direction of north-south. Therefore, heavy damages are obtained in structural elements of these regions. Furthermore, crushing regions are observed in some cracking zones of the mosque, it is assumed that regions between these crushing zones are reached to local collapse mechanism. The mechanism are developed due to movement in direction of north-south of right and left aisle walls which neighbor to middle aisle in 2 and 3 axes. Furthermore, another collapse mechanism are seen in the B axis, this mechanism are also developed due to movement of central hall in direction of north-south. As a results, structural elements of the mosque in direction of north-south should be strengthened for conservation works of this significant historical mosque.

References

[1] Ching, F. D., Jarzombek, M. M., and Prakash, V. "*A global history of architecture*". John Wiley & Sons, New Jersey. 2010.

[2] Proske, D., and van Gelder, P. "*Safety of historical arch bridges*". Springer-Verlag. 2009. https://doi.oeg/10.1007/978-3-540-77618-5

[3] Sunkar, M., and Aksoy, H. S. "Adobe buildings damaged during Kovancılar (Elazığ) earthquake on March 8, 2010 and their earthquake resistances". *KSCE Journal of Civil Engineering*, 19(4), pp. 943–51. 2015. https://doi.org/10.1007/s12205-012-0400-8

[4] Sayın, E., Yön, B., Calayır, Y., and Karaton, M. "Failures of masonry and adobe buildings during the June 23, 2011 Maden-(Elazığ) earthquake in Turkey". *Engineering Failure Analysis*, 34, pp. 779–91. 2013. https://doi.org/10.1016/j.engfailanal.2012.10.016

[5] Ramos, L. F., and Lourenço, P. B. "Modeling and vulnerability of historical city centers in seismic areas: a case study in Lisbon". *Engineering Structures*, 26(9), pp. 1295–1310. 2004. https://doi.org/10.1016/j.engstruct.2004.04.008

[6]. Betti, M., and Vignoli, A. "Numerical assessment of the static and seismic behaviour of the basilica of Santa Maria all'Impruneta (Italy)". *Construction and Building Materials*, 25(12), pp. 4308–4324. 2011. https://doi.org/10.1016/j.conbuildmat.2010.12.028

[7]. Brandonisio, G., Lucibello, G., Mele, E., and De Luca, A. "Damage and performance evaluation of masonry churches in the 2009 L'Aquila earthquake". *Engineering Failure Analysis*, 34, pp. 693–714. 2013. https://doi.org/10.1016/j.engfailanal.2013.01.021

[8] Saloustros, S., Pelà, L., Roca, P., and Portal, J. "Numerical analysis of structural damage in the church of the Poblet monastery". *Engineering Failure Analysis*, 48, 41–61. 2015. https://doi.org/10.1016/j.engfailanal.2014.10.015

[9] DLH 2007. "Earthquake Technical Regulations Relating to Coastal, Harbor, Railway and Airport Constructions". Ankara, Turkey (in Turkish): Ministry of Transportation Turkey.

[10] Meskouris, K., Butenweg, C., Mistler, M., and Kuhlmann, W. "Seismic behaviour of historic masonry buildings". In: *Proceeding of 7th National Congress on Mechanics of HSTAM*. Chania, Crete, Greece. 2004. pp. 37–49.

[11] Willam, K. J., and E. P., Warnke. "Constitutive model for the triaxial behavior of concrete". In *Proceedings of the International Association for Bridge and Structural Engineering*, 19(1), pp. 1–30. 1975.

[12] ANSYS. 2015. Finite Element Software. Houston, TX, USA: Swanson Analysis System. Inc.

[13] Zienkiewicz, O. C., and R. L. Taylor. "*The finite element method*". Vol. 3. McGraw-Hill, New York, 1977.

[14] Akurgal, E., and Hilber L. "*The art and architecture of Turkey"*. Rizzoli International Publications, New York. 1980.

[15] Poole, R. W., and Farmer, I. W. "Consistency and repeatability of Schmidt hammer rebound data during field testing". *International Journal of Rock Mechanics and Mining Sciences & Geomechanics*, 17(3), pp. 167–171. 1980. https://doi.org/10.1016/0148-9062(80)91363-7

[16] Aksoy, H. S., and Yılmaz, U. "Evaluation of the relationships between Schmidt rebound number and strength of rocks". In: *3rd International Conference on New Developments in Soil Mechanics and Geotechnical Engineering*. Jun. 28–30. 2012. pp. 525–530. https://zm2012.neu.edu.tr/ZM2012%20DVD/Soil%20Characterisation/065.pdf

[17] Kahveci, A. E. "A study on investigation of using bazalt Stone as construction material in Diyarbakır region". MSc dissertation, Süleyman-Demirel University, Isparta, Turkey. 2008.

[18] Yılmaz, I., and Sendir, H. "Correlation of Schmidt hardness with unconfined compressive strength and Young's modulus in gypsum from Sivas (Turkey)". *Engineering Geology*, 66(3), pp. 211–219. 2002. https://doi.org/10.1016/S0013-7952(02)00041-8

[19] Katz, O., Reches, Z., and Roegiers, J. C. „Evaluation of mechanical rock properties using a Schmidt Hammer". *International Journal of Rock Mechanics and Mining Sciences*, 37(4), pp. 723–28. 2000. https://doi.org/10.1016/S1365-1609(00)00004-6

[20] Aydin, A., and Basu A. "The Schmidt hammer in rock material characterization". *Engineering Geology*, 81(1), pp. 1–14. 2005. https://doi.org/10.1016/j.enggeo.2005.06.006

[21] Kahraman, S. "Evaluation of simple methods for assessing the uniaxial compressive strength of rock". *International Journal of Rock Mechanics and Mining Sciences*, 38(7), pp. 981–994. 2001. https://doi.org/10.1016/S1365-1609(01)00039-9

[22] Buyuksagis, I. S., and Goktan, R. M. "The effect of Schmidt hammer type on uniaxial compressive strength prediction of rock". *International Journal of Rock Mechanics and Mining Sciences*, 44(2), pp. 299–307. 2007. https://doi.org/10.1016/j.ijrmms.2006.07.008

[23] Yagiz, S. "Predicting uniaxial compressive strength, modulus of elasticity and index properties of rocks using the Schmidt hammer". *Bulletin of engineering geology and the environment*, 68(1), pp. 55–63. 2009. https://doi.org/10.1007/s10064-008-0172-z

[24] Karaveziroglou, M., Papayianni, J., and Penelis, G. "Mortars and grouts in restoration of Roman and Byzantine monuments". In: *Proceeding Compatible Materials for the protection of European Cultural Heritage*. 2. Athens: Technical Chamber of Greece. pp. 219–245. 1998.

[25] ENV 1996-1-1. Eurocode 6: Design of Masonry Structures—Part 1-1: General Rules for Reinforced and Unreinforced Masonry Structures. Brussels, Belgium: Comit Europen de Normalisation. 2005. https://law.resource.org/pub/eu/eurocode/en.1996.1.1.2005.pdf

[26] Ersoy, H.Y. "Composite material". Literature press. Istambul. 2001. (in Turkish)

[27] Oral, M. B., Reilinger, R., and Toksoz, R. "Deformation of the Anatolian block as deduced from GPS measurements". Transactions, American Geophysical Union, EOS, 73(120): 7–19. 1992.

[28] Reilinger, R. E., McClusky, S. C., Oral, M. B., King, R. W., Toksoz, M. N., Barka, A. A., Kinik, I., Lenk, O., Sanli, I. "Global Positioning System measurements of present-day crustal movements in the Arabia-Africa-Eurasia plate collision zone". *Journal of Geophysical Research: Solid Earth*, 102(B5), pp. 9983–99. 1997. 10.1029/96JB03736

[29] AFAD, Republic of Turkey Prime Ministry Disaster and Emergency Management Authority (2016) http://www.deprem.gov.tr/sarbis/Veritabani/Tarihsel.aspx

[30] Cetin, H., Güneyli, H., and Mayer, L. "Paleoseismology of the Palu–Lake Hazar segment of the East Anatolian fault zone, Turkey". *Tectonophysics*, 374(3), pp. 163–197. 2003. https://doi.org/10.1016/j.tecto.2003.08.003

[31] SeismoArtif. 2013. Seismic Artificial Earthquake Generating Software. Pavia, Italy: Seismosoft.Inc.